Transient Angle Stability of Paralleled Synchronous and Virtual Synchronous Generators in Islanded Microgrids

Huijie Cheng, Zhikang Shuai, *Senior Member, IEEE*, Chao Shen, Xuan Liu, *Member, IEEE*, Zuyi Li, *Senior Member, IEEE*, and Z. John Shen, *Fellow, IEEE*

***Abstract*—With the development of virtual synchronous generator (VSG) techniques, parallel operations of synchronous generators (SGs) and VSGs become increasingly common in a microgrid. The differences between paralleled systems will affect the transient stability of the system, which probably threatens stable operation of the system, especially under fault conditions. In this article, the transient angle stability of a paralleled synchronous and virtual synchronous generators (SG-VSG) system is investigated by comparing it with that of the paralleled VSGs system. It is observed that the paralleled SG-VSG system is more prone to transient instability due to the differences between their speed governors. Then, a control method is proposed to improve the transient stability of the paralleled SG-VSG system. Furthermore, a Lyapunov method is employed to establish the nonlinear model of islanded microgrid, by which the attraction domain of paralleled system is quantified. The hardware-in-loop experiment is performed to validate the theoretical analysis.**

***Index Terms*—Islanded microgrid, lyapunov method, paralleled system, synchronous generator (SG), transient angle stability, virtual synchronous generator (VSG).**

I. Introduction

TO ADDRESS the environmental pollution and energy crisis, an increasing portion of distributed energy resources (DERs) are being integrated into conventional power systems via power electronic converters, which leads to a huge change in the structure of power systems [1]–[4]. Because of flexibility and controllability of power electronics, microgrids are experiencing a rapid development and can operate both in islanding and grid-connected modes [5], [6]. However, it is vulnerable to disturbances caused by intermittency and uncertainty of renewable energies due to lack of inertia, damping, and spinning reserve capacity of power electronic converters, which poses considerable challenges in the secure operation. To resolve those problems, virtual synchronous generators (VSGs) are designed [7], [8].

With an increasing number of VSGs connected to the microgrid, the stability problems are aroused extensive attentions and have been chiefly focused on that of a single VSG and paralleled VSGs [8]–[12]. However, VSGs are a type of inverters with low overcurrent capabilities and thus, are susceptible to physical damages and need to be protected through the control switching or even forced outages under severe disturbances [13]. Hence, reliable power sources are essential to maintain the secure level of frequency and voltage of an islanded microgrid. Synchronous generator (SG)-based DERs are one of typical reliable power sources and widely used in a Consortium for Electric Reliability Technology Solutions microgrid [14], [15]. Consequently, a paralleled synchronous and virtual synchronous generators (SG-VSG) system exists in microgrids and its stability problems are needed to be investigated as well, especially under large disturbances. More importantly, the transient instability mechanism of paralleled SG-VSG systems is more complicated than that of a single VSG or paralleled VSGs, which leads to the difficulty of system planning and designing, and even threatens the system security.

Prior studies have been primarily carried out to analyze the transient stability of a single VSG and paralleled VSGs. A single grid-connected VSG is prone to instability because the reactive power control loop reduces the internal voltage amplitude of a VSG through Q–V curve during severe faults [16]. Although droop-control and VSG-control methods resemble greatly, their differences lie in that VSG-control methods own the links of virtual inertia and virtual damping over droop-control methods [17], [18]. A swing equation of droop-control inverter is built and a Lyapunov function was derived to evaluate the stability margin [19]. Transient stability of droop-controlled inverters is deteriorated during faults due to the existence of a current limiter [20], [21]. The full-order nonlinear model of droop-controlled inverters is established by means of the Takagi–Sugeno (TS) fuzzy model-based Lyapunov method. Then, the accuracy and validity of reduced order models are discussed in replicating the performance of the full-order model [22]. Nevertheless, the

Manuscript received May 21, 2019; revised September 9, 2019 and December 6, 2019; accepted January 4, 2020. Date of publication January 8, 2020; date of current version April 22, 2020. This work was supported in part by the National Natural Science Foundation of China under Grant 51977066, and in part by Hunan Provincial Innovation Foundation for Postgraduate CX20190299. Recommended for publication by Associate Editor M. Molinas. *(Corresponding author: Zhikang Shuai.)*

H. Cheng, Z. Shuai, C. Shen, and X. Liu are with the College of Electrical and Information Engineering, Hunan University, Changsha 410006, China (e-mail: jessycheng@hnu.edu.cn; szk@hnu.edu.cn; shenchaos1992@163.com; xliu@hnu.edu.cn).

Z. Li and Z. J. Shen are with the Department of Electrical and Computer Engineering, Illinois Institute of Technology, Chicago, IL 60616 USA (e-mail: lizu@iit.edu; zjohnshen@gmail.com).

Color versions of one or more of the figures in this article are available online at https://ieeexplore.ieee.org.

Digital Object Identifier 10.1109/TPEL.2020.2965152

studies mentioned above focus on the transient stability of a single grid-connected inverter. Generally, large quantities of inverter-based DERs operate in parallel to scale up the total generation capacity in microgrids. Thus, it is necessary to investigate the transient stability of multiple paralleled VSGs. Robust stability of paralleled VSGs is analyzed in [9] and characteristics of power oscillation for paralleled VSGs are studied in [10] and [11]. However, the analysis and mechanism on transient stability are not covered. Alipoor *et al*. in [12] propose a transient stability assessment for paralleled VSGs, but no theoretical analysis is provided for transient stability mechanism of the system.

Several research works have been reported on analysis of transient characteristics for paralleled SG-VSG systems. The work in [23] experimentally investigates the transient power-sharing characteristics of paralleled SG-VSG systems. A transient energy analysis is adopted to assess transient stability of a paralleled SG-VSG system in [24]. Transient response between SGs and droop-controlled inverters is studied based on simulation results [25]. However, those studies mentioned above lack a theoretical analysis to reveal transient stability mechanism of paralleled SG-VSG systems. The work in [26] investigates the stability of microgrids and interactions between SG-based and inverter-based DERs under islanded conditions. Nevertheless, it is of narrow limitation to develop large-signal stability of the system by means of small-signal methods. The cascading collapse occurs in a large-scale microgrid during extreme events, because of the slow response of SG-based DERs [27]. However, essential explanations are lacked to understand the instability mechanism of the system. Thus, there is an urgent need to investigate the transient stability mechanism of the paralleled SG-VSG system. Based on the theoretical analysis, a control method can be designed to improve the transient stability of the system.

To guarantee secure operation of VSGs during a fault, varieties of fault ride through control methods are proposed in [13], [28], and [29]. Those control methods primarily contribute to limiting the fault current, but the effects on transient stability of paralleled systems are not discussed. An enhanced control strategy is added in VSGs by reducing the reference active power, which can improve transient stability of the system [16]. The work in [21] proposes a stability enhanced P–f droop control to prevent the inverter from transient instability under large disturbances. However, both control methods are designed for the improvement of transient stability of grid-connected inverters, but might not be suitable for parallel operation of SGs and inverters in an islanded microgrid. Hence, a novel control method is needed to be considered for enhancing the transient stability of the paralleled SG-VSG system. Then, a Lyapunov function is derived to evaluate the effectiveness of the proposed method and estimate stability regions of the system. Here, the approach for deriving the function is based on a TS fuzzy model which is useful for modeling nonlinear systems with multiplication, division, exponential, or square root nonlinearities [22], [30]. Besides, linear matrix inequalities (LMI) technique is needed to maximize the size of the stability region [31], [32].

This article aims to investigate transient angle stability of a paralleled SG-VSG system. It is found that the paralleled SG-VSG system is more likely to lose stability than the paralleled VSGs system under serious faults, due to their differences. Then, a new control method is introduced to enhance the transient stability of the system. Moreover, a Lyapunov function based on the TS fuzzy model is derived to quantify transient stability margins of paralleled systems. The main contributions of this article are summarized as follows.

1) According to the deduced swing equations, the difference of speed governors is found between the paralleled VSGs system and the paralleled SG-VSG system.
2) The instability mechanism of paralleled SG-VSG system is revealed and comparison of stable operation capability between two paralleled systems is discussed.
3) A stability-enhanced control method is proposed to improve the transient stability of the paralleled SG-VSG system by changing the equivalent input torque of the system.
4) The influences of different parameters on the attraction domains of the paralleled SG-VSG system are analyzed.

The remainder of this article is organized as follows. In Section II, swing equations of both paralleled VSGs system and paralleled SG-VSG system are established, and the transient instability mechanisms of paralleled systems are explored. In Section III, a stability-enhanced control method is designed and a Lyapunov function is deduced to evaluate the transient stability of the paralleled SG-VSG system. Experimental results are obtained to verify the theoretical analysis in Section IV. Section V concludes this article.

II. Transient Stability Analysis of Paralleled Systems

In this section, swing equations of a paralleled SG-VSG system and a paralleled VSGs system are established to discuss the differences between two paralleled systems. Then, the transient instability mechanism of paralleled SG-VSG can be revealed through power–angle (P–δ) curves.

A. Swing Equation of Paralleled Systems

As depicted in Fig. 1(a), the control parts of a SG consist of an automatic voltage regulator (AVR) and governor. The AVR and speed governor regulate the terminal voltage and mechanical speed, respectively [33]. The SG is connected to the bus through transformer and transmission lines. L_T represents the equivalent transformer inductance. R_l and L_l are the equivalent resistance and inductance of transmission line l, respectively. Fig. 1(b) shows the control block of a VSG which is comprised of active- and reactive power control loops. To be specific, the active power control loop is to emulate rotor motion equations and regulate active power, while the reactive power control loop is to control terminal voltage and regulate reactive power [7]. L_f is the filter inductance of VSGs.

The swing equation of SGs is as follows [33]:

$$J_g \frac{d\omega_g}{dt} = T_{mg} - T_{eg} - D_g \omega_g \tag{1}$$

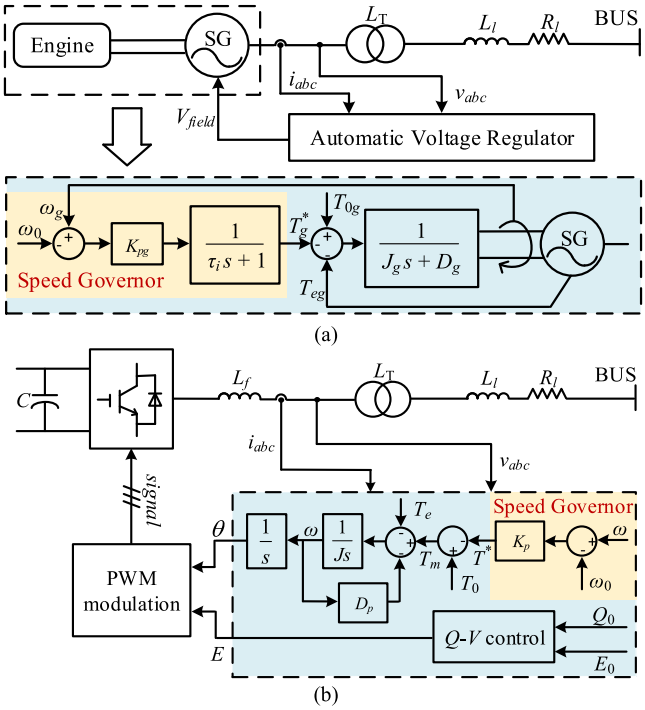

Fig. 1. Control blocks. (a) SG. (b) VSG.

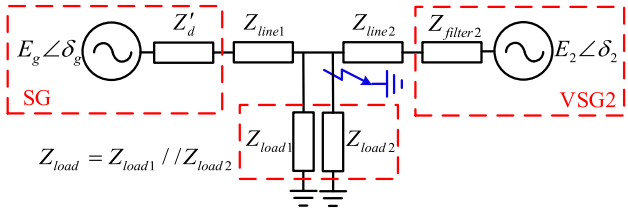

Fig. 2. Equivalent circuit of a paralleled SG-VSG system.

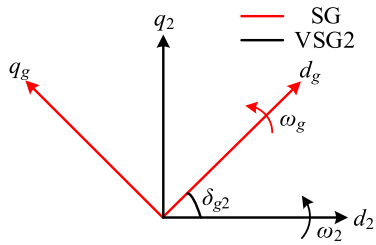

Fig. 3. Reference frames of SG and VSG2.

where J_g and D_g represent the inertia constant and damping coefficient of SG, respectively. ω_g is the rotor angular frequency of SG. T_{eg} is the SG's electromagnetic torque and T_{mg} is generated by the speed governor, which can be expressed as follows:

$$T_{mg} = T_{0g} - T_g^* \tag{2}$$

$$\frac{dT_{mg}}{dt} = \frac{1}{\tau_i}[T_{0g} - K_{pg}(\omega_g - \omega_0) - T_{mg}] \tag{3}$$

where K_{pg} is the control parameters of the speed governor. τ_i and ω_0 are the time-delay constant and reference angular frequency, respectively. T_{0g} represents the reference input torque. $T_g^* = K_{pg}(\omega_g - \omega_0)$.

Combining (1)–(3), there is

$$J_g\frac{d\omega_g}{dt} = T_{0g} - K_{pg}(\omega_g - \omega_0) - \tau_i\frac{dT_{mg}}{dt} - T_{eg} - D_g\omega_g. \tag{4}$$

The swing equation of VSGs is as follows [15]:

$$J\frac{d\omega}{dt} = T_m - T_e - D_p\omega \tag{5}$$

where J and D_p denote the virtual inertia and virtual damping coefficient of VSG, respectively. ω is the virtual rotor angular frequency of VSG. T_e is the VSG's output torque and T_m is generated by the governor, which can be written as follows:

$$T_m = T_0 - T^* \tag{6}$$

where T_0 represents the reference input torque. $T^* = K_p(\omega–\omega_0)$.

According to (5) and (6), there is

$$J\frac{d\omega}{dt} = T_0 - K_p(\omega - \omega_0) - T_e - D_p\omega. \tag{7}$$

According to (4) and (7), it is found that speed governors are the main differences between SGs and VSGs.

Fig. 2 shows the equivalent circuit of a paralleled SG-VSG system. A three-phase short-circuit fault occurs at the load2, and then the load2 is cut off to clear the fault. An SG can be regarded as a voltage source in series with an impedance [23]. Z'_d is equal to jx'_d and x'_d is the transient reactance. Also, a VSG can be regarded as a voltage source in series with an impedance [16]. E_2 and δ_2 are the amplitude and phase of internal voltage of VSG2. Z_{fliter2} represent the filter impedance of VSG2. Z_{load} represent the load impedance. Z_{linek} is the total impedance between the export of SG/VSG and the bus, which can be calculated by the following:

$$Z_{\text{linek}} = R_l + j\omega_0\left(L_l + L_T\right). \tag{8}$$

The voltage-oriented reference frames of SG and VSG2 are shown in Fig. 3, where the axis (d_g–q_g) and axis (d_2–q_2) are their frames rotating at a frequency of ω_g and ω_2, respectively. The axis (d_2–q_2) is chosen as the common reference frame for the paralleled SG-VSG system. δ_{g2} is the angle difference between the SG and VSG, which can be expressed as follows:

$$\dot{\delta}_{g2} = \omega_g - \omega_2. \tag{9}$$

Fig. 4 shows the equivalent circuit of a paralleled VSGs system. E_k and δ_k are the amplitude and phase of internal voltage of VSG, respectively ($k = 1, 2$). Z_{fliterk} represents the filter impedance of VSG. The reference frames of VSG1 and VSG2 are shown in Fig. 5, where the axis1 (d_1–q_1) and axis2 (d_2–q_2) are their reference frames rotating at a frequency of ω_1 and ω_2, respectively. Assuming that the angular acceleration of VSG1

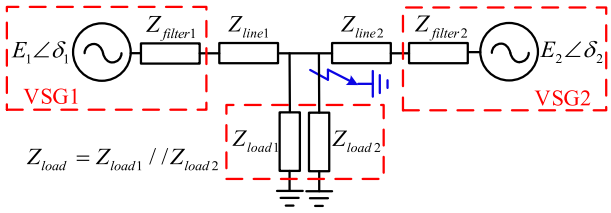

Fig. 4. Equivalent circuit of a paralleled VSGs system.

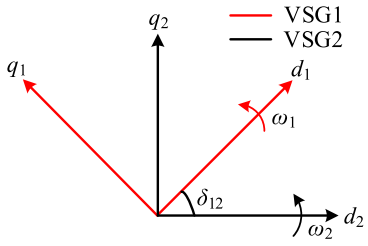

Fig. 5. Reference frame of VSG1 and VSG2.

is greater than that of VSG2 during a fault, the axis (d_2–q_2) is selected as the common reference frame in the paralleled VSGs system. Hence, δ_{12} is the angle difference between VSG1 and VSG2, which leads to

$$\dot{\delta}_{12} = \omega_1 - \omega_2. \tag{10}$$

The swing equations of the paralleled SG-VSG system and the paralleled VSGs system are presented as equations (B.8) and (B.10) in Appendix B, respectively. Obviously, speed governors are the main differences between two paralleled systems.

B. Transient Angle Stability Analysis of Paralleled Systems

As analyzed above, the main difference between two paralleled systems is speed governors. This part will investigate the effect of the difference on the transient angle stability of the paralleled SG-VSG system.

Assuming that D_g/J_g and D_{p1}/J_1 are equal to D_{p2}/J_2; K_{pg}/J_g and K_{p1}/J_1 are as large as K_{p2}/J_2, (B.8) and (B.10) can be changed into

$$J_{eqg}\frac{d^2\delta'_{g2}}{dt^2} = \left(T_{Mg} - J_{eqg}\frac{D_{p2}}{J_2}\omega_{g2}\right) - T_{\text{emg}}\sin\delta'_{g2} \tag{11}$$

$$J_{\text{eq}}\frac{d^2\delta'_{12}}{dt^2} = \left(T_M - J_{\text{eq}}\frac{D_{p2}}{J_2}\omega_{12}\right) - T_{em}\sin\delta'_{12}. \tag{12}$$

The damping link belongs to a part of the equivalent input torque, since it owns a similar function with a speed governor based on (11) and (12). The equivalent input torques of both paralleled systems can be rewritten as follows:

$$T'_{Mg} = \frac{J_2T_{0g} - J_gT_{02}}{J_g + J_2} - \frac{J_2E_g^2G_{gg} - J_gE_2^2G_{22}}{(J_g + J_2)\omega_0} - J_{eqg}\frac{D_{e2}}{J_2}\omega_{g2} - \frac{J_2}{J_g + J_2}\tau_i\frac{dT_{mg}}{dt} \tag{13}$$

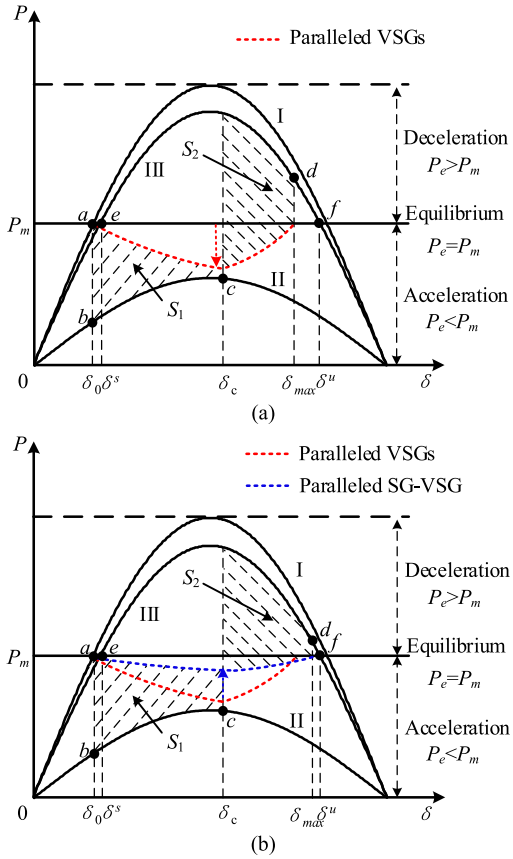

Fig. 6. P–δ curve of paralleled systems. (a) Paralleled VSGs system. (b) Paralleled SG-VSG system.

$$T'_M = \frac{J_2T_{01} - J_1T_{02}}{J_1 + J_2} - \frac{J_2E_1^2G_{11} - J_1E_2^2G_{22}}{(J_1 + J_2)\omega_0} - J_{\text{eq}}\frac{D_{e2}}{J_2}\omega_{12} \tag{14}$$

where D_{e2} denotes the equivalent damping coefficient and $D_{e2} = D_{p2} + K_{p2}$.

To analyze the effects of the differences on the transient angle stability of the paralleled SG-VSG system, the transient stability of the paralleled VSGs system is first discussed. During the fault, the input torque of the paralleled VSGs system can be adjusted via speed governors and damping links. Assuming that the angular acceleration of VSG1 is greater than that of VSG2 during a fault, the angular frequency of VSG1 is higher than that of VSG2. Thus, the term $-(J_{eq}D_{e2}/J_2)\omega_{12}$ in (14) is negative. The input power will be continually changed unless the system reaches steady state. The P–δ curve of the paralleled VSGs system is shown in Fig. 6(a), where the red dashed line represents the input power of the paralleled VSGs system during the fault; Curves I, II, and III describe the relationship between the output power P and the power angle δ of the paralleled system during the prefault, fault, and postfault, respectively. Before subjecting to the fault, the paralleled system initially operates at the stable equilibrium point a. The operating point moves from point a to b, when a short-circuit fault occurs. In this case, the virtual rotor of the paralleled system keeps accelerating and thus δ successively increases according to (12). From (14), the

input torque of the paralleled VSGs system is decreased and the acceleration area S_1 is decreased. δ decelerates since the output power is larger than the input power, after the fault is cleared at point c. The acceleration area S_1 is equal to the deceleration area S_2, when the paralleled system operates at point d. Points e and f are the stable and unstable equilibrium point, respectively. The paralleled system is stable if the power angle δ^u of point f is larger than $\delta_{\max}$ of point d.

As analyzed above, the predominant differences between two paralleled systems are speed governors, which can influence the transient angle stability of the paralleled SG-VSG system. From (13) and (14), their difference only affects the input torque of paralleled systems. The difference of speed governors is represented by the term $-[J_2\tau_i/(J_g + J_2)](dT_{mg}/dt)$. It is known that the transient angle instability of the paralleled system is intrinsically caused by the imbalance between the input and output powers. Thus, it is crucial to discuss the influence of their difference on the input torque of the paralleled system during a fault.

The difference of speed governors is reflected in that of time-delay links. The effects of time-delay link of an SG on transient angle stability of the system are analyzed as follows. Since the SG's input torque T_{mg} decreases by means of speed governors, $-[J_2\tau_i/(J_g + J_2)](dT_{mg}/dt)$ in (13) is positive and thus the input torque of the paralleled SG-VSG system is larger than that of the paralleled VSGs system. The rotor of SG starts to decelerate, when the fault is cleared. T_{mg} increases and then $-[J_2\tau_i/(J_g + J_2)](dT_{mg}/dt)$ is negative, which prevents T_{mg} from increasing. In the early stage of fault clearance, the input power of the paralleled SG-VSG system is still larger than that of the paralleled VSGs system, as shown in Fig. 6(b). The blue dashed line stands for the input power of the paralleled SG-VSG system when the difference of speed governors is considered. Obviously, the input power changes with the variation of SG's angular frequency. Compared to the paralleled VSGs system, the acceleration area of the paralleled SG-VSG system increases, and its deceleration area decreases. Thus, the paralleled SG-VSGs system becomes more prone to instability than the paralleled VSGs system. In this section, transient angle stability of the system is analyzed under three-phase symmetrical faults. For the analysis of system transient stability under asymmetric faults, the system is needed to be separated into positive, negative, and zero sequence networks [33].

III. Stability-Enhanced Control and Transient Stability Estimation

In this section, a new method is proposed to improve the transient angle stability based on the instability mechanism analysis of a paralleled SG-VSG system. Besides, a Lyapunov function is derived to quantify the stability margin of paralleled SG-VSG system.

A. Stability-Enhanced VSG Control

As discussed in Section II, the input power of the paralleled SG-VSG system increases more than that of the paralleled VSGs system, since paralleled SG-VSG system owns a supplementary time-delay link compared with the paralleled VSG system. That would lead to both a larger acceleration area and a smaller deceleration area, which reduces the stability margin of the system. Namely, the angle instability is caused by the sustained imbalance between the input power and output power during a fault. Thus, the transient angle stability of the system can be enhanced by reduction of the input power.

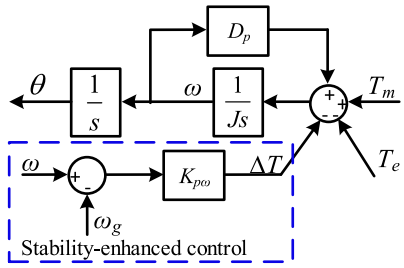

Fig. 7. Diagram of the stability-enhanced control.

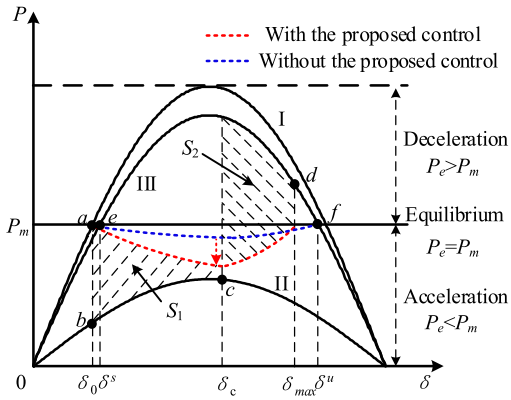

Fig. 8. P–δ curve of the paralleled SG-VSG system with the stability-enhanced control.

Fig. 7 gives the block diagram of the stability-enhanced control. To achieve it, the steps are as follows: the angular frequency of SG is collected to be fed into VSG control; the difference of angular frequency between SG and VSG is sent into a proportional controller; an additional torque is produced to adjust the input torque. The additional torque can be expressed by

$$\Delta T = K_{p\omega}(\omega - \omega_g) \tag{15}$$

where $K_{p\omega}$ is the stability-enhanced coefficient.

Fig. 8 shows the P–δ curve of the paralleled SG-VSG system with the stability-enhanced control. The control method does not contribute when the angular frequency of SG is equal to that of VSG in steady state. As is known in Section II, the angular frequency of SG is larger than that of VSG during a short-circuit fault. Hence, ΔT is negative according to (15). The equivalent input torque of the paralleled SG-VSG system is decreased from (13) and thus the stability margin of the system is increased.

B. Lyapunov Function Based on TS Fuzzy Model

A TS fuzzy model is used to derive a Lyapunov function which can be applied to the estimation of attraction domains of the system [22]. The Lyapunov function is constructed by the steps as follows.

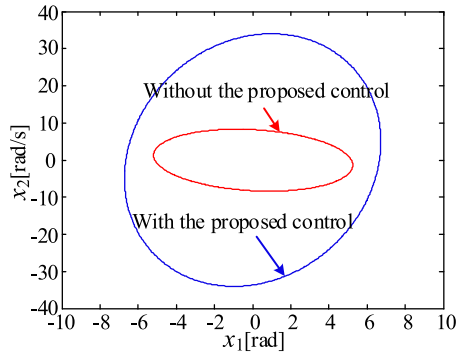

Fig. 9. Estimated attraction domain of paralleled systems projected on the x_1–x_2 plane, where x_1 is δ_{g2}–δ_{g20} and x_2 is ω_g–ω_{g0}.

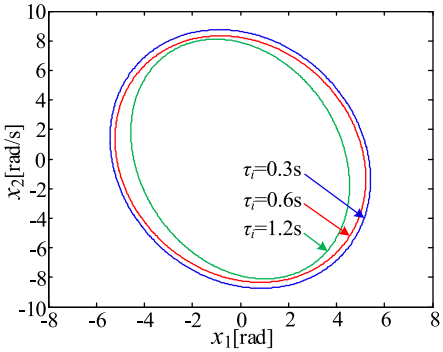

Fig. 10. Estimated attraction domain with variations of τ_i.

Step 1: Defining the nonlinear system as $\dot{x} = A(x)x$ and establishing a nonlinear matrix function $A(x)$.

Step 2: Calculating the minimum and maximum values for each nonlinear quantity in $A(x)$. Thus, 2^r matrices A_i are obtained when there are r nonlinear quantities.

Step 3: Obtaining a matrix M which satisfies the LMI:

$$\begin{cases} M = M^T > 0 \\ A_i^T M + M A_i < 0. \end{cases} \tag{16}$$

Step 4: Constructing the Lyapunov function, which is expressed as follows:

$$V(x) = x^T M x. \tag{17}$$

TS fuzzy model-based Lyapunov functions of the paralleled SG-VSG system are detailed in Appendix C. The attraction domains of paralleled systems can be evaluated. Fig. 9 shows the attraction domains of paralleled systems projected on the x_1–x_2 plane, where the state variables x_1 is δ_{g2}–δ_{g20} and x_2 is ω_g–ω_{g0}. The system can regain its equilibrium when it is initialized within the estimated domain. It can be seen that the estimated attraction domain of the paralleled SG-VSG system with the proposed method is larger than that of the paralleled SG-VSG system without the proposed method, which is consistent with the theoretical results.

C. Effect of Different Parameters on Attraction Domain

The effects of different parameters on the attraction domain of the paralleled SG-VSG system are investigated in this part.

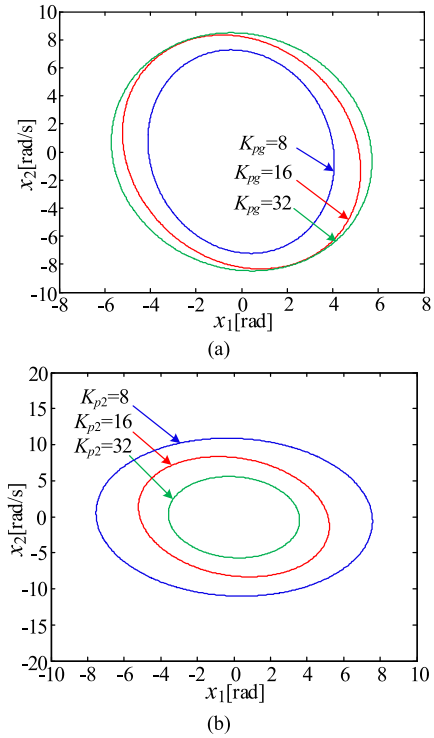

Fig. 11. Estimated attraction domain of the paralleled SG-VSG system. (a) Variations of K_{pg}, (b) Variations of K_{p2}.

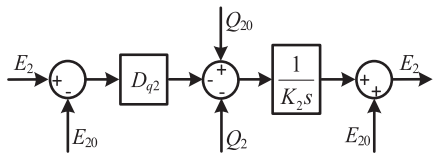

Fig. 12. Reactive power control loop of VSG2.

1) Effect of Time-Delay Constant τ_i: The effect of time-delay constant on attraction domain is analyzed with τ_i varied from 0.3 to 1.2 s, as depicted in Fig. 10. It is shown that the attraction domain decreases with the increase of the time-delay constant. That is, a larger time-delay constant is not conducive to the system stability. A larger time-delay constant leads to slower change in the input power during faults, which leads to the rapid increases of power angle and thus deteriorates the transient angle stability of the system.

2) Effect of Proportional Controller Parameter K_{pg} and K_{p2}: Fig. 11 shows the estimated attraction domains with different K_{pg} and K_{p2}. The results show that a larger K_{pg} or a smaller K_{p2} is more beneficial to the transient stability of the paralleled SG-VSG system. As indicated in Fig. 6(d), a larger K_{pg} or a smaller K_{p2} would lead to a smaller acceleration area during a fault and a larger deceleration area during a postfault. Namely, a larger K_{pg} or a smaller K_{p2} would help the system to return back to stability after the clearance of a fault.

3) Effect of Reactive Power Control Loop of VSG2: The reactive power control loop of VSG2 is shown in Fig. 12 [16], [17], which can be expressed as follows:

$$K_2 \frac{dE_2}{dt} = Q_{02} - Q_2 - D_{q2}(E_2 - E_{02}) \tag{18}$$

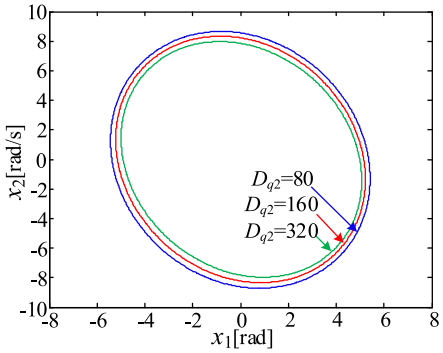

Fig. 13. Estimated attraction domain with variations of D_{q2}.

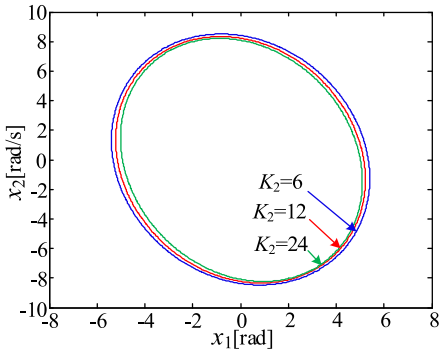

Fig. 14. Estimated attraction domain with variations of K_2.

where K_2 and D_{q2} are the voltage integral coefficient and Q–V coefficient, respectively. Q_2 and Q_{02} represent the reactive power and reference reactive power, respectively. E_{02} is the reference voltage.

Obviously, the effects of reactive power control loop on the system stability can be illustrated by estimating attraction domains with variations of the coefficients D_{q2} and K_2. The Q–V coefficient D_{q2} increases from 80 to 320 and the result is given in Fig. 13. A larger D_{q2} leads to a smaller estimated attraction domain, which would deteriorate the system stability. Fig. 14 depicts that the estimated attraction domain of the system will be enlarged with a smaller K_2.

IV. Validations

In this section, the simulation results verify the accuracy of analytical models of both paralleled systems in Section II. Then, the control hardware-in-loop experiments are implemented to validate the correctness of theoretical analysis and the effectiveness of the proposed method.

A. Simulation Results

The simulations are carried out to validate the accuracy of analytical models in Section II. Fig. 15 shows the time-domain responses of angular frequencies and active powers of VSG1 and VSG2 in the paralleled VSGs system. The fault duration is 0.7 s. The red dashed lines represent waveforms of angular frequencies and active powers of the analytical model. The blue

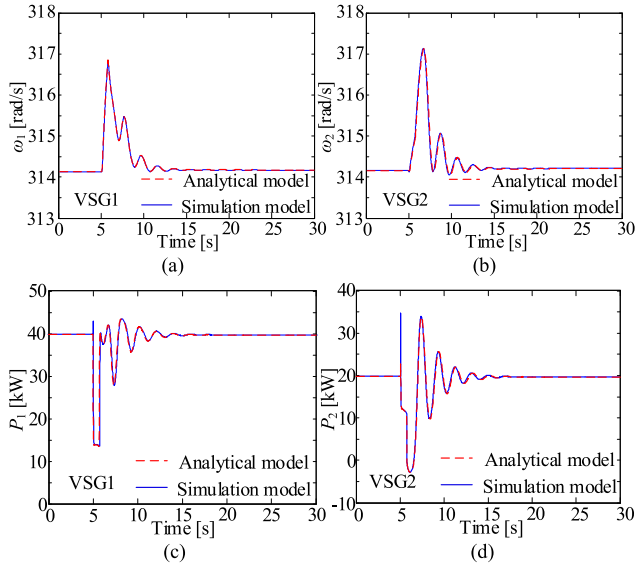

Fig. 15. Comparison of time-domain evaluation between the analytical models and simulation models in paralleled VSGs system when the fault duration is 0.7 s. (a) Angular frequency of VSG1. (b) Angular frequency of VSG2. (c) Active power of VSG1. (d) Active power of VSG2.

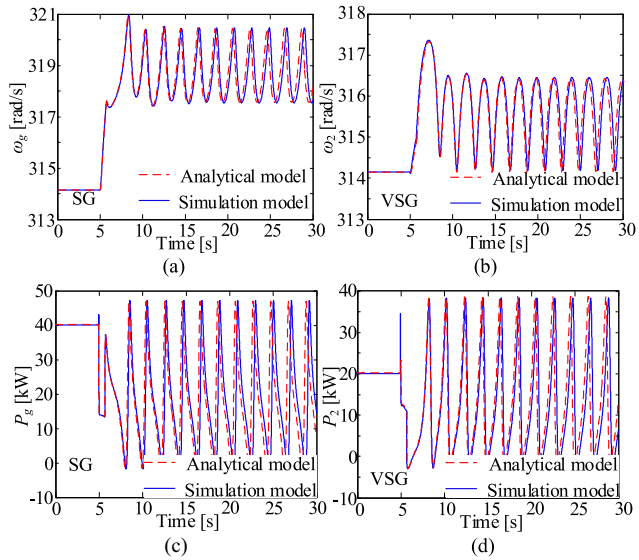

Fig. 16. Comparison of time-domain evaluation between the analytical models and simulation models in the paralleled SG-VSG system when the fault duration is 0.7 s. (a) Angular frequency of SG. (b) Angular frequency of VSG. (c) Active power of SG. (d) Active power of VSG.

solid lines stand for waveforms of angular frequencies and active powers of the simulation model. Obviously, similar responses of angular frequencies are obtained from both models during prefault, fault, and postfault. The amplitude of active power of simulation model is larger than that of the analytical model at the moment that a symmetrical fault occurs, while there are similar transient responses of active powers during fault and postfault. Namely, the analytical model of the paralleled VSGs system can capture the transient performance well.

Fig. 16 depicts the time-domain evolutions of angular frequencies and active powers of SG and VSG in the paralleled

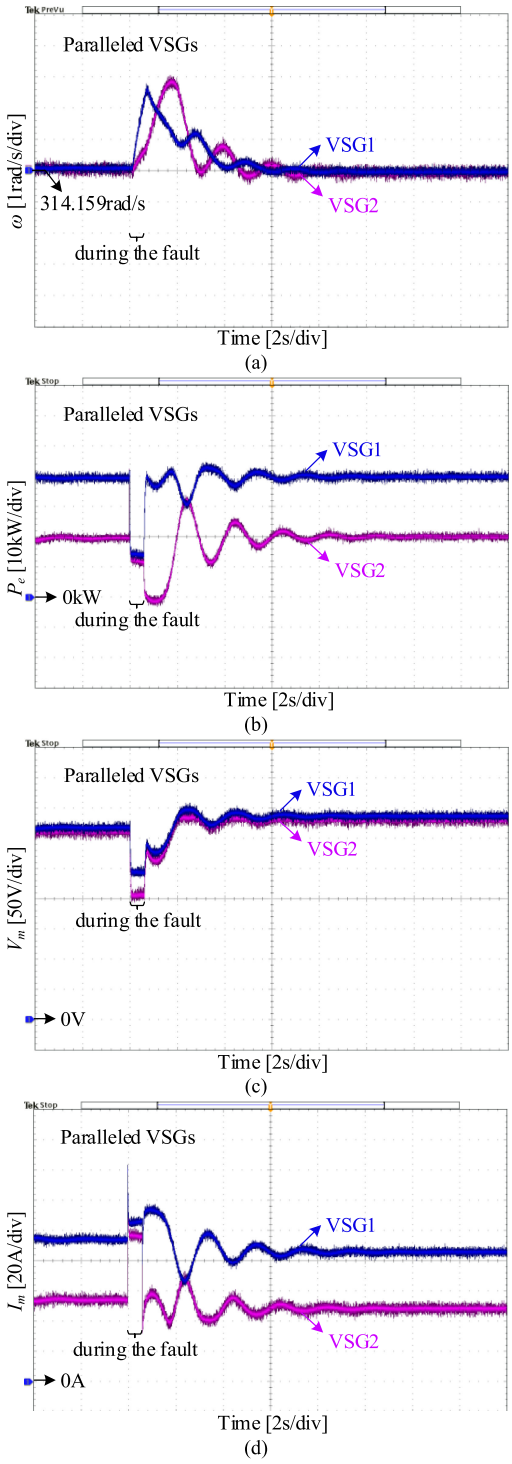

Fig. 17. Experiment results of paralleled VSGs system when the fault duration is 0.62 s. (a) Angular frequency of VSG1 and VSG2. (b) Active power of VSG1 and VSG2. (c) Voltage magnitude of VSG1 and VSG2. (d) Current magnitude of VSG1 and VSG2.

SG-VSG system. At the same fault duration, the paralleled SG-VSG system loses its stability and the angular frequencies and active powers of both models oscillate. It can be noticed that the transient behavior of the analytical model matches well with that of the simulation model during the fault. After the fault is cleared, both models have similar transient responses on

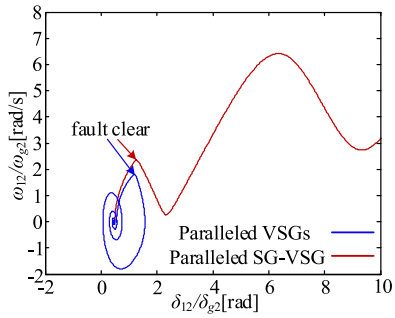

Fig. 18. Angular frequency versus power angle trajectory of two paralleled systems when the fault duration is 0.62 s.

the 10 s time scale. Thus, the analytical model of the paralleled SG-VSG system can be used to analyze transient angle stability of the system.

B. Experimental Results: Paralleled Systems

The control hardware-in-loop experiments are carried out to verify the correctness of the theoretical analysis. Figs. 2 and 4 show the study systems, and the control blocks are depicted in Fig. 1. Detailed parameters are given in Table I of Appendix A.

1) Paralleled VSGs System: Fig. 17 shows the experimental results of the paralleled VSGs system when the fault duration is 0.62 s. ω and P_e represent the angular frequency and active power, respectively. V_m and I_m are the voltage magnitude and current magnitude.

As depicted in Fig. 17, the angular acceleration of VSG1 is greater than that of VSG2 during the fault, which is coincident with the theoretical assumptions. The angle difference between VSG1 and VSG2 is sustainably increased. The active power and voltage magnitude of VSG1 and VSG2 are decreased while the current magnitude is suddenly increased. After the fault is cleared, the angular speeds of two VSGs are finally equal and reach a stable equilibrium point. Besides, the active power, voltage, and current remain stable.

2) Paralleled SG-VSG System: Fig. 18 shows the angular frequency versus power angle trajectory of two paralleled systems when the duration of the short-circuit fault is 0.62 s. ω_{12} and δ_{12} are the angular frequency and angle difference between two VSGs. ω_{g2} and δ_{g2} are the angular frequency and angle difference between the SG and the VSG. The power angle of the paralleled VSGs system returns to a stable equilibrium point. However, the power angle of the paralleled SG-VSG system cannot get to an equilibrium point and system state variables diverge, which is consistent with the theoretical results.

The corresponding experimental results of paralleled SG-VSG system are illustrated in Fig. 19. The angular frequencies of SG and VSG2 keep oscillating after the fault is cleared at 4.62 s. Consequently, the angle difference between SG and VSG2 will be continuously increased. Namely, the system loses transient angle stability. The voltage, current, and active power continually fluctuate in this condition, as depicted in Fig. 19(b)–(d).

In summary, the experimental results of two paralleled systems are compared after the fault is cleared. The transient angle

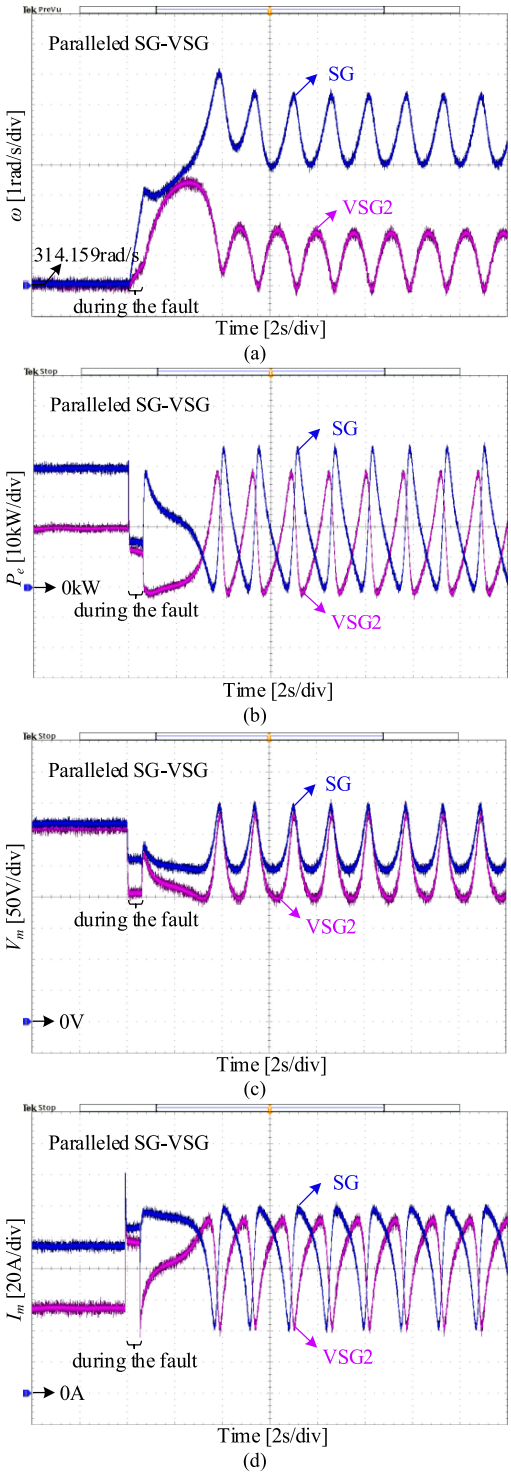

Fig. 19. Experiment results of the paralleled SG-VSG system when the fault duration is 0.62 s. (a) Angular frequency of SG and VSG2. (b) Active power of SG and VSG2. (c) Voltage magnitude of SG and VSG2. (d) Current magnitude of SG and VSG2.

instability occurs in the paralleled SG-VSG system, which accompanies with the phenomenon of increase of sustained angle between the SG and the VSG. Simultaneously, the voltage, current, and power are oscillating. Nevertheless, the paralleled

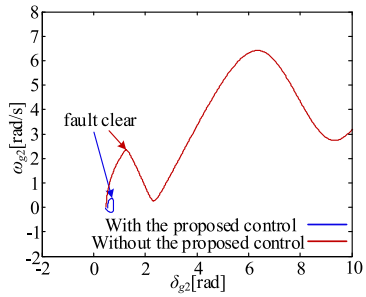

Fig. 20. Angular frequency versus power angle trajectory with or without the proposed method when the fault duration is 0.62 s.

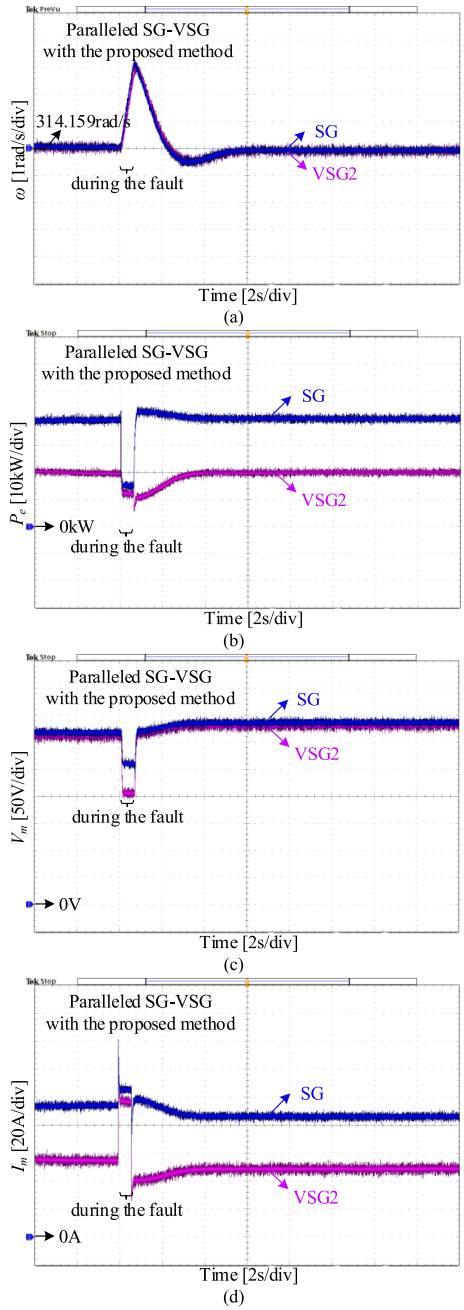

Fig. 21. Experiment results of the paralleled SG-VSG system with the proposed method when the fault duration is 0.62 s. (a) Angular frequency of SG and VSG2. (b) Active power of SG and VSG2. (c) Voltage magnitude of SG and VSG2. (d) Current magnitude of SG and VSG2.

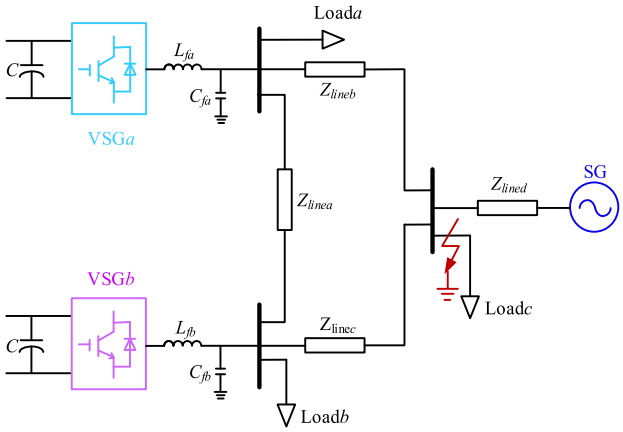

Fig. 22. Topology of parallel operation of a SG and two VSGs in an islanded microgrid.

VSGs system can restore stability with the stable voltage, current, and power. It can be proved that the differences between two paralleled systems aggravate the transient instability of the paralleled SG-VSG system.

3) Paralleled SG-VSG System With the Proposed Method: The stability-enhanced control is added in VSG2 to improve the transient stability of the paralleled SG-VSG system. The stability-enhanced coefficient $K_{p\omega}$ is 100. Angular frequency versus power angle trajectory with or without the proposed method is shown in Fig. 20. It can be seen that the system loses stability without the proposed method, while it can return to the stable equilibrium point with the proposed method after the fault is cleared at 4.62 s. The proposed method can change the fault trajectory of the studied system because it slows down the acceleration process and speeds up the deceleration process by balancing the input active power and the output active power. Furthermore, effectiveness of the proposed method to enhance the transient stability is demonstrated by experiment results.

From Fig. 21(a), the angular frequency of VSG2 can track that of SG well and thus the angle difference between SG and VSG2 is relatively smaller during the fault. The angular frequencies of SG and VSG2 are stable and the system is in steady state after the fault clearance. The voltage, current, and active power remain stale under the circumstances, as depicted in Fig. 21(b)–(d). Thus, the proposed method can improve the transient stability of the paralleled SG-VSG system.

C. Experimental Results: Parallel Operation of an SG and Two VSGs in an Islanded Microgrid

To further validate the effectiveness of the proposed method, the transient response of parallel operation of an SG and two VSGs in an islanded is investigated and its topology is presented in Fig. 22. A short-circuit fault occurs at load$a$ and the fault duration is 2 s. Detailed parameters are shown in Table II of Appendix A.

The angular frequencies of SG and two VSGs are shown in Fig. 23(a). Obviously, those angular frequencies keep oscillating and the system loses transient angle stability after the fault clearance. Moreover, the active power of SG and two VSGs is

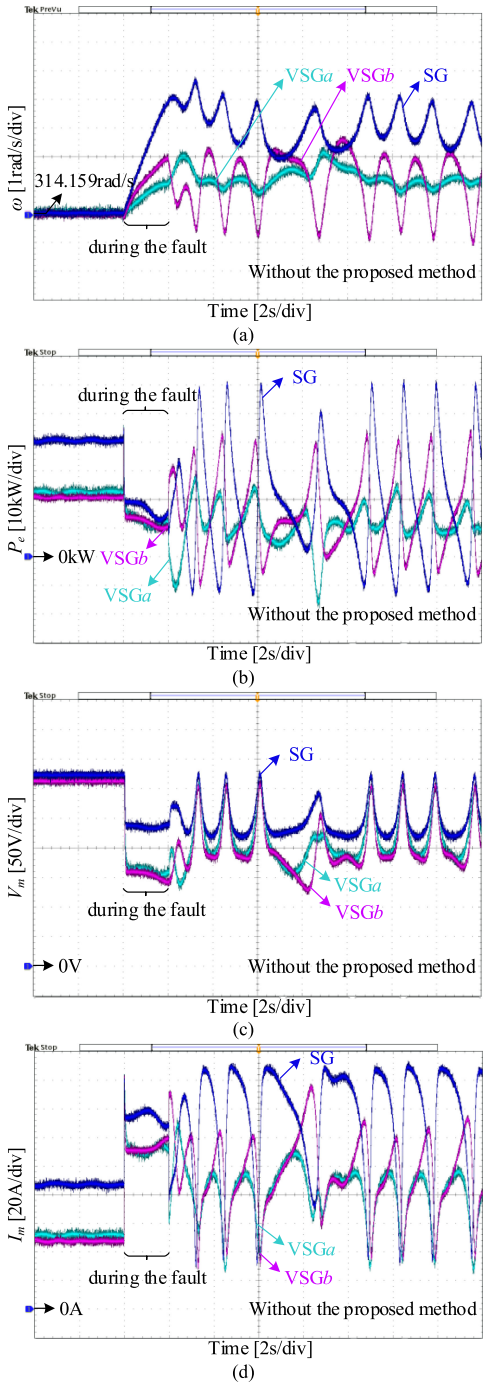

Fig. 23. Experiment results of parallel operation of a SG and two VSGs when the fault duration is 2 s. (a) Angular frequency of a SG and two VSGs. (b) Active power of a SG and two VSGs. (c) Voltage magnitude of a SG and two VSGs. (d) Current magnitude of a SG and two VSGs.

dramatically oscillating, as depicted in Fig. 23(b). Their voltage and current are unstable, which is illustrated in Fig. 23(c) and (d). That stability problem deteriorates the system responses and results in failure of the system recovery when the system is subjected to large disturbances.

Fig. 24 shows the experiment results of the system with the proposed method. Clearly, the angular frequencies of SG and two VSGs are approximately the same and continuously increase during the fault. Those angular frequencies start to

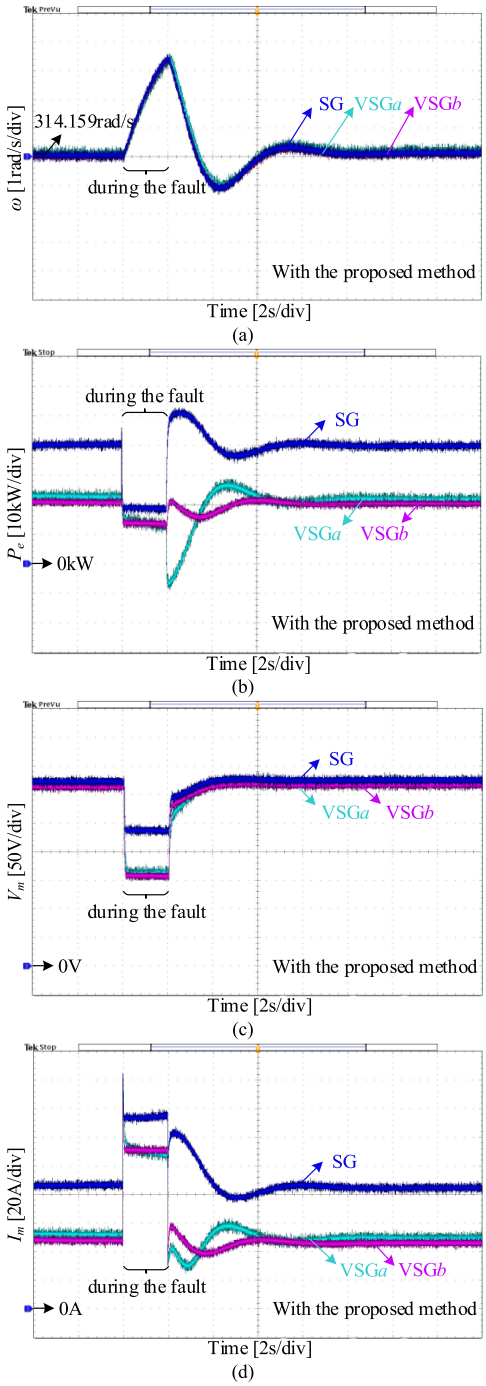

Fig. 24. Experiment results of parallel operation of an SG and two VSGs with the proposed method when the fault duration is 2 s. (a) Angular frequency of an SG and two VSGs. (b) Active power of a SG and two VSGs. (c) Voltage magnitude of a SG and two VSGs. (d) Current magnitude of a SG and two VSGs.

restore stability when the fault is cleared at 6 s. Accordingly, the active power, voltage, and current of SG and two VSGs are also in a steady state. That is, the system can remain in synchronism after large disturbance.

From the results in Figs. 23 and 24, it can be observed that the proposed method can effectively enhance the system stability under large disturbances and guarantee the secure operation of the system.

V. Conclusion

In this article, the transient stability of two islanded systems is investigated in the context of paralleled VSGs and paralleled SG-VSG. The differences of two systems are discussed and the instability mechanisms of the paralleled SG-VSG system are elaborated through P–δ curves. Based on the theoretical analysis, a novel control method is proposed to improve the transient stability of the paralleled SG-VSG system. Furthermore, a Lyapunov function is proposed based on TS fuzzy model to quantify the transient stability of the paralleled system.

1) The transient angle instability of the paralleled SG-VSG system is worse aggravated by the time delay of SG's speed governor under large disturbances, compared to that of the paralleled VSGs system.
2) The transient stability of the paralleled SG-VSG system can be enhanced by decreasing the input active power, because transient angle instability results from the imbalance between the input power and output power.
3) The SG with a larger time-delay constant is easier to drive a paralleled SG-VSG system into the unstable region during a fault. The estimated attraction domain of the paralleled SG-VSG system is reduced under the condition of SG with a smaller proportional controller parameter. However, the VSG with a smaller proportional controller parameter is more beneficial for transient stability of the system.
4) The attraction domains of the paralleled SG-VSG system are estimated with variations of the voltage integral coefficient and Q–V coefficient of VSG, which quantifies the effects of reactive power control loop on the system stability. The system is more likely to lose stability with a larger voltage integral coefficient or a larger Q–V coefficient of VSG.

Appendix A

TABLE I
System Parameters

Parameters	Value	Parameters	Value
P_{01}	40 kW	P_{02}	20 kW
J_1	15.0224	J_2	15.0224
K_{p1}	16	K_{p2}	16
D_{p1}	0.01	D_{p2}	0.01
P_{0g}	40 kW	τ_i	0.6 s
J_g	15.0224	K_{pg}	16
D_g	0.01	x'_d	0.19 p.u.
x_{filter}	0.19 p.u.	Z_{line1}	0.16+j0.25 p.u.
Z_{line2}	0.16+j0.25 p.u.	Z_{load}	0.58 p.u.
Q_{01}	5 kVar	Q_{02}	5 kVar
K_1	12	K_2	12
D_{q1}	160.77	D_{q2}	160.77

TABLE II
SYSTEM PARAMETERS

Parameters	Value	Parameters	Value
P_{0g}	40 kW	τ_i	0.6 s
J_g	15.0224	K_{pg}	16
D_g	0.01	x'_d	0.17 p.u.
P_{0a}	20 kW	P_{0b}	20 kW
J_a	15.0224	J_b	5.0224
K_{pa}	16	K_{pb}	8
D_{pa}	0.01	D_{pb}	0.01
Q_{0a}	5 kVar	Q_{0b}	5 kVar
K_a	24	K_b	12
D_{qa}	160.77	D_{qb}	160.77
$x_{filtera}$	0.19 p.u.	$x_{filterb}$	0.19 p.u.
Z_{linea}	0.08+j0.21 p.u.	Z_{lineb}	0.08+j0.21 p.u.
Z_{lineb}	0.08+j0.21 p.u.	Z_{lined}	0.16+j0.25 p.u.

APPENDIX B

1) SWING EQUATION OF THE PARALLELED SG-VSG SYSTEM

According to [8] and [33], the dynamics of inductors can be ignored those are in the faster time scale compared with the dynamics of power control loop and mechanical rotor. The active power of SG and VSG can be calculated by [30]

$$P_g = E_g^2 G_{gg} + E_g E_2 |Y_{g2}| \cos(\delta_{g2} + \phi_{g2}) \tag{B.1}$$

$$P_2 = E_2^2 G_{22} + E_g E_2 |Y_{g2}| \cos(\delta_{g2} - \phi_{g2}) \tag{B.2}$$

where G_{gg} and B_{gg} are the conductance and susceptance of Y_{gg}. G_{22} and B_{22} are the conductance and susceptance of Y_{22}. $|Y_{g2}|$ and ϕ_{g2} are the amplitude and phase of Y_{g2}

$$\begin{cases} Y_{gg} = Y_g (Y_2 + Y_3) / (Y_g + Y_2 + Y_3) \\ Y_{g2} = -Y_g Y_2 / (Y_g + Y_2 + Y_3) \\ Y_{22} = Y_2 (Y_g + Y_3) / (Y_g + Y_2 + Y_3) \end{cases} \tag{B.3}$$

where

$$\begin{cases} Y_g = 1/Z_{tg} \\ Y_2 = 1/Z_{t2} \\ Y_3 = 1/Z_{\text{load}} \end{cases} \tag{B.4}$$

where $Z_{tg} = Z'_d + Z_{line2}$ and $Z_{t2} = Z_{filter2} + Z_{line2}$.

From (4), (7), (B.1), and (B.2), the swing equations of SG and VSG can be derived as follows:

$$J_g \frac{d^2\delta_g}{dt^2} = T'_{mg} - \frac{E_g E_2 |Y_{g2}|}{\omega_{g0}} \sin\delta_g^t - D_g \omega_g \tag{B.5}$$

$$J_2 \frac{d^2\delta_2}{dt^2} = T'_2 - \frac{E_g E_2 |Y_{g2}|}{\omega_{20}} \sin\delta_g^t - D_{p2} \omega_2 \tag{B.6}$$

where ω_{g0} and ω_{20} are equal, which can be represented by ω_0

$$\begin{cases} T'_{mg} = T_{0g} - \frac{E_g^2 G_{gg}}{\omega_0} - K_{pg}(\omega_g - \omega_0) - \tau_i \frac{dT_{mg}}{dt} \\ T'_2 = T_{02} - \frac{E_2^2 G_{22}}{\omega_0} - K_{p2}(\omega_2 - \omega_0) \\ \delta_g^t = \delta_{g2} + \phi_{g2} - 90^\circ \\ \delta_2^t = \delta_{g2} - \phi_{g2} - 90^\circ. \end{cases} \tag{B.7}$$

Combining (B.5) and (B.6), the swing equation of the paralleled VSGs system can be deduced as follows [30]:

$$J_{eqg} \frac{d^2\delta'_{g2}}{dt^2} = T_{Mg} - T_{emg} \sin\delta'_{g2} - J_{eqg} \left(\frac{D_g}{J_g}\omega_g - \frac{D_{p2}}{J_2}\omega_2 \right) \tag{B.8}$$

where $d^2\delta'_{g2}/dt^2$ is the relative angular acceleration between SG and VSG. $J_{\text{eq\_}g}$ is the equivalent inertia constant of the paralleled SG-VSG system. T_{Mg} and $T_{emg}\sin\delta'_{g2}$ are the equivalent input and output torque of the paralleled SG-VSG system, respectively

$$\begin{cases} J_{eqg} = \frac{J_g J_2}{J_g + J_2} \\ \delta'_{g2} = \delta_{g2} - \gamma_g \\ \gamma_g = -\text{arccot}(\frac{J_g - J_2}{J_g + J_2}\cot\phi_{g2}) - 90^\circ \\ T_{Mg} = \frac{J_2 T_{mg} - J_g T_{m2}}{J_g + J_2} - \frac{J_2 E_g^2 G_{gg} - J_g E_2^2 G_{22}}{(J_g + J_2)\omega_0} \\ T_{mg} = T_{0g} - K_{pg}(\omega_g - \omega_0) - \tau_i \frac{dT_{mg}}{dt} \\ T_{m2} = T_{02} - K_{p2}(\omega_2 - \omega_0) \\ T_{emg} = \frac{E_g E_2 |Y_{g2}| \sqrt{J_g^2 + J_2^2 - 2J_g J_2 \cos 2\phi_{g2}}}{(J_g + J_2)\omega_0}. \end{cases} \tag{B.9}$$

2) SWING EQUATION OF THE PARALLELED VSGs SYSTEM

Similarly, the swing equation of the paralleled VSGs system can be expressed by

$$J_{eq} \frac{d^2\delta'_{12}}{dt^2} = T_M - T_{em} \sin\delta'_{12} - J_{eq} \left(\frac{D_{p1}}{J_1}\omega_1 - \frac{D_{p2}}{J_2}\omega_2 \right) \tag{B.10}$$

where $d^2\delta'_{12}/dt^2$ is the relative angular acceleration between VSG1 and VSG2. J_{eq} is the equivalent inertia of the paralleled VSGs system. T_M and $T_{em}\sin\delta'_{12}$ are the equivalent input- and output torque of the paralleled VSGs system. The variables mentioned above are presented as follows:

$$\begin{cases} J_{eq} = \frac{J_1 J_2}{J_1 + J_2} \\ \delta'_{12} = \delta_{12} - \gamma \\ \gamma = -\text{arccot}(\frac{J_1 - J_2}{J_1 + J_2} cot\phi_{12}) - 90^\circ \\ T_M = \frac{J_2 T_{01} - J_1 T_{02}}{J_1 + J_2} - \frac{J_2 E_1^2 G_{11} - J_1 E_2^2 G_{22}}{(J_1 + J_2)\omega_0} \\ T_{m1} = T_{01} - K_{p1}(\omega_1 - \omega_0) \\ T_{m2} = T_{02} - K_{p2}(\omega_2 - \omega_0) \\ T_{em} = \frac{E_1 E_2 |Y_{12}| \sqrt{J_1^2 + J_2^2 - 2J_1 J_2 \cos 2\phi_{12}}}{(J_1 + J_2)\omega_0} \end{cases} \tag{B.11}$$

where G_{11} and B_{11} are the conductance and susceptance of Y_{11}. G_{22} and B_{22} are the conductance and susceptance of Y_{22}. $|Y_{12}|$ and ϕ_{12} are the amplitude and phase of Y_{12}

$$\begin{cases} Y_{11} = Y_1 (Y_2 + Y_3) / (Y_1 + Y_2 + Y_3) \\ Y_{12} = -Y_1 Y_2 / (Y_1 + Y_2 + Y_3) \\ Y_{22} = Y_2 (Y_1 + Y_3) / (Y_1 + Y_2 + Y_3) \end{cases} \tag{B.12}$$

where Y_1, Y_2, and Y_3 are as follows:

$$\begin{cases} Y_1 = 1/Z_{t1} \\ Y_2 = 1/Z_{t2} \\ Y_3 = 1/Z_{\text{load}} \end{cases} \tag{B.13}$$

where Z_{tk} is equal to the sum of $Z_{\text{filter}k}$ and $Z_{\text{line}k}$.

APPENDIX C

1) PARALLELED SG-VSG SYSTEM

The paralleled SG-VSG system can be modeled as follows [8], [33]:

$$\begin{cases}
\dot{x}_1 = x_2 - x_6 \\
\dot{x}_2 = \frac{1}{J_1}\{[1.5\left(L'_d - L_q\right) f\left(x_2\right) f\left(x_4\right) f\left(x_5\right) - D_{eg}]\, x_2 \\
\quad -1.5 f\left(x_2\right) f\left(x_5\right) x_3 + 1.5\omega_{g0} \\
\quad \left(L'_d - L_q\right) I_{1q0} f\left(x_2\right) x_4 \\
\quad -1.5\left[E'_{q0} f\left(x_2\right) - \omega_{g0}\left(L'_d - L_q\right) f\left(x_2\right) f\left(x_4\right)\right] \\
\quad x_5 + x_{10}\} \\
\dot{x}_3 = \frac{1}{T'_{d0}}\left[-x_3 - \left(x_d - x'_d\right) x_4\right] \\
\dot{x}_4 = \frac{R_{\text{load}}}{L_{\text{line1}}}\Big[\left(\sin\delta_{g20} f\left(x_8\right) - \cos\delta_{g20} f\left(x_9\right)\right) x_1 \\
\quad + \frac{L_{\text{line1}}+L_q}{R_{\text{load}}} f\left(x_5\right) x_2 - \left(1 + \frac{R_{tg}}{R_{\text{load}}}\right) x_4 \\
\quad + \frac{L_{\text{line1}}+L_q}{R_{\text{load}}}\omega_{g0} x_5 - \cos\delta_{g20} x_8 - \sin\delta_{g20} x_9\Big] \\
\dot{x}_5 = \frac{R_{\text{load}}}{L_{line1}}\Big[\left(\sin\delta_{g20} f\left(x_9\right) + \cos\delta_{g20} f\left(x_8\right)\right) x_1 \\
\quad - \frac{L_{tg}}{R_{\text{load}}} f\left(x_4\right) x_2 + \frac{1}{R_{\text{load}}} x_3 - \frac{L_{tg}}{R_{\text{load}}}\omega_{10} x_4 \\
\quad - \left(1 + \frac{R_{tg}}{R_{\text{load}}}\right) x_5 + \sin\delta_{g20} x_8 - \cos\delta_{g20} x_9\Big] \\
\dot{x}_6 = \frac{1}{J_2}\left(-D_{e2} x_6 - 1.5 f\left(x_6\right) f\left(x_9\right) x_7 - 1.5 E_{20} f\left(x_6\right) x_9\right) \\
\dot{x}_7 = \frac{1}{K_2}\left[\left(-D_{q2} - 1.5 f\left(x_8\right)\right) x_7 - 1.5 E_{20} x_8\right] \\
\dot{x}_8 = \frac{R_{\text{load}}}{L_{t2}}\Big[\left(\sin\delta_{g20} f\left(x_4\right) + \cos\delta_{g20} f\left(x_5\right)\right) x_1 \\
\quad - \cos\delta_{g20} x_4 + \sin\delta_{g20} x_5 + \frac{L_{t2}}{R_{\text{load}}} f\left(x_9\right) x_6 \\
\quad - \left(1 + \frac{R_{t2}}{R_{\text{load}}}\right) x_8 + \frac{L_{t2}}{R_{\text{load}}}\omega_{20} x_9\Big] \\
\dot{x}_9 = \frac{R_{\text{load}}}{L_{t2}}\Big[\left(-\cos\delta_{g20} f\left(x_4\right) + \sin\delta_{g20} f\left(x_5\right)\right) x_1 \\
\quad - \sin\delta_{g20} x_4 - \cos\delta_{g20} x_5 - \frac{L_{t2}}{R_{\text{load}}} f\left(x_8\right) x_6 \\
\quad + \frac{1}{R_{\text{load}}} x_7 - \frac{L_{t2}}{R_{\text{load}}}\omega_{20} x_8 - \left(1 + \frac{R_{t2}}{R_{\text{load}}}\right) x_9\Big] \\
\dot{x}_{10} = \frac{1}{\tau_i}\left(-K_p x_2 - x_{10}\right)
\end{cases} \tag{C.1}$$

with

$$\begin{cases}
x_1 = \delta_{g2} - \delta_{g20}, x_2 = \omega_g - \omega_{g0} \\
x_3 = E'_q - E'_{q0}, x_4 = I_{1d} - I_{1d0} \\
x_5 = I_{1q} - I_{1q0}, x_6 = \omega_2 - \omega_{20} \\
x_7 = E_2 - E_{20}, x_8 = I_{2d} - I_{2d0} \\
x_9 = I_{2q} - I_{2q0}, x_{10} = T_{mg} - T_{mg0}
\end{cases} \tag{C.2}$$

$$\begin{cases}
f\left(x_2\right) = \frac{1}{x_2 + \omega_{g0}}, \quad f\left(x_4\right) = x_4 + I_{1d0}, f\left(x_5\right) = x_5 + I_{1q0} \\
f\left(x_6\right) = \frac{1}{x_6 + \omega_{20}}, \quad f\left(x_8\right) = x_8 + I_{2d0}, f\left(x_9\right) = x_9 + I_{2q0}
\end{cases} \tag{C.3}$$

where D_{eg} equals to the sum of K_{pg} and D_g. x_d and T'_{d0} are the d-axis synchronous reactance and the d-axis open-circuit transient time constant. E'_q is the internal voltage of SG. D_{e2} is equivalent to the sum of K_{p2} and D_{p2}. I_{kd} and I_{kq} represent the d-axis and q-axis components of line current. The subscript "0" refers to the steady-state operating point.

Based on the above model, the system is expressed as $\dot{x} = A(x)x$ with six nonlinear quantities. Then, the Lyapunov function can be constructed by following the steps in Section III-B.

2) PARALLELED SG-VSG SYSTEM WITH THE PROPOSED METHOD

The paralleled SG-VSG system with the proposed method can be modeled as follows [8], [33]: eq. (C.4) shown at the bottom of this page, with

$$\begin{cases}
x_1 = \delta_{g2} - \delta_{g20}, x_2 = \omega_g - \omega_{g0} \\
x_3 = E'_q - E'_{q0}, x_4 = I_{1d} - I_{1d0} \\
x_5 = I_{1q} - I_{1q0}, x_6 = \omega_2 - \omega_{20} \\
x_7 = E_2 - E_{20}, x_8 = I_{2d} - I_{2d0} \\
x_9 = I_{2q} - I_{2q0}, x_{10} = T_{mg} - T_{mg0}
\end{cases} \tag{C.5}$$

$$\begin{cases}
\dot{x}_1 = x_2 - x_6 \\
\dot{x}_2 = \frac{1}{J_1}\{[1.5\left(L'_d - L_q\right) f\left(x_2\right) f\left(x_4\right) f\left(x_5\right) - D_{eg}]\, x_2 - 1.5 f\left(x_2\right) f\left(x_5\right) x_3 + 1.5\omega_{g0}\left(L'_d - L_q\right) I_{1q0} f\left(x_2\right) x_4 \\
\quad -1.5\left[E'_{q0} f\left(x_2\right) - \omega_{g0}\left(L'_d - L_q\right) f\left(x_2\right) f\left(x_4\right)\right] x_5 + x_{10}\} \\
\dot{x}_3 = \frac{1}{T'_{d0}}\left[-x_3 - \left(x_d - x'_d\right) x_4\right] \\
\dot{x}_4 = \frac{R_{\text{load}}}{L_{\text{line1}}}\Big[\left(\sin\delta_{g20} f\left(x_8\right) - \cos\delta_{g20} f\left(x_9\right)\right) x_1 + \frac{L_{\text{line1}}+L_q}{R_{\text{load}}} f\left(x_5\right) x_2 - \left(1 + \frac{R_{tg}}{R_{\text{load}}}\right) x_4 \\
\quad + \frac{L_{line1}+L_q}{R_{\text{load}}}\omega_{g0} x_5 - \cos\delta_{g20} x_8 - \sin\delta_{g20} x_9\Big] \\
\dot{x}_5 = \frac{R_{\text{load}}}{L_{\text{line1}}}\Big[\left(\sin\delta_{g20} f\left(x_9\right) + \cos\delta_{g20} f\left(x_8\right)\right) x_1 - \frac{L_{tg}}{R_{\text{load}}} f\left(x_4\right) x_2 + \frac{1}{R_{\text{load}}} x_3 - \frac{L_{tg}}{R_{\text{load}}}\omega_{10} x_4 \\
\quad - \left(1 + \frac{R_{tg}}{R_{\text{load}}}\right) x_5 + \sin\delta_{g20} x_8 - \cos\delta_{g20} x_9\Big] \\
\dot{x}_6 = \frac{1}{J_2}\left(K_{p\omega} x_2 - \left(D_{e2} + K_{p\omega}\right) x_6 - 1.5 f\left(x_6\right) f\left(x_9\right) x_7 - 1.5 E_{20} f\left(x_6\right) x_9\right) \\
\dot{x}_7 = \frac{1}{K_2}\left[\left(-D_{q2} - 1.5 f\left(x_8\right)\right) x_7 - 1.5 E_{20} x_8\right] \\
\dot{x}_8 = \frac{R_{\text{load}}}{L_{t2}}\Big[\left(\sin\delta_{g20} f\left(x_4\right) + \cos\delta_{g20} f\left(x_5\right)\right) x_1 - \cos\delta_{g20} x_4 + \sin\delta_{g20} x_5 + \frac{L_{t2}}{R_{\text{load}}} f\left(x_9\right) x_6 - \left(1 + \frac{R_{t2}}{R_{\text{load}}}\right) x_8 + \frac{L_{t2}}{R_{\text{load}}}\omega_{20} x_9\Big] \\
\dot{x}_9 = \frac{R_{\text{load}}}{L_{t2}}\Big[\left(-\cos\delta_{g20} f\left(x_4\right) + \sin\delta_{g20} f\left(x_5\right)\right) x_1 - sin\delta_{g20} x_4 - \cos\delta_{g20} x_5 - \frac{L_{t2}}{R_{\text{load}}} f\left(x_8\right) x_6 \\
\quad + \frac{1}{R_{\text{load}}} x_7 - \frac{L_{t2}}{R_{\text{load}}}\omega_{20} x_8 - \left(1 + \frac{R_{t2}}{R_{\text{load}}}\right) x_9\Big] \\
\dot{x}_{10} = \frac{1}{\tau_i}\left(-K_p x_2 - x_{10}\right)
\end{cases} \tag{C.4}$$

$$\begin{cases} f(x_2) = \frac{1}{x_2+\omega_{g0}}, f(x_4) = x_4 + I_{1d0}, f(x_5) = x_5 + I_{1q0} \\ f(x_6) = \frac{1}{x_6+\omega_{20}}, f(x_8) = x_8 + I_{2d0}, f(x_9) = x_9 + I_{2q0} \end{cases}. \tag{C.6}$$

Similarly, the system is represented as $\dot{x} = A(x)x$ with six nonlinear quantities. Then, the Lyapunov function can be constructed by following the steps in Section III-B.

REFERENCES

[1] Z. Shuai, W. Huang, X. Shen, Y. Li, X. Zhang, and Z. Shen, "A maximum power loading factor (MPLF) control strategy for distributed secondary frequency regulation of islanded microgrid," *IEEE Trans. Power Electron.*, vol. 34, no. 3, pp. 2275–2291, Mar. 2019.

[2] M. Firuzi, A. Roosta, and M. Gitizadeh, "Stability analysis and decentralized control of inverter-based ac microgrid," *Protection Control Modern Power Syst.*, vol. 4, no. 6, pp. 1–24, Mar. 2019.

[3] Z. Shuai, Y. Peng, J. Guerrero, Y. Li, and Z. Shen, "Transient response analysis of inverter-based microgrids under unbalanced conditions using dynamic phasor model," *IEEE Trans. Ind. Electron.*, vol. 66, no. 4, pp. 2868–2879, Apr. 2019.

[4] Y. Peng, Z. Shuai, X. Liu, Z. Li, J. M. Guerrero, and Z. J. Shen, "Modeling and stability analysis of inverter-based microgrid under harmonic conditions," *IEEE Trans. Smart Grid*, to be published, doi: 10.1109/TSG.2019.2936041.

[5] B. Singh, G. Pathak, and B. Panigrahi, "Seamless transfer of renewable-based microgrid between utility grid and diesel generator," *IEEE Trans. Power Electron.*, vol. 33, no. 10, pp. 8427–8437, Oct. 2018.

[6] Y. Peng, Z. Shuai, J. M. Guerrero, Y. Li, A. Luo, and Z. J. Shen, "Performance improvement of the unbalanced voltage compensation in islanded microgrid based on small-signal analysis," *IEEE Trans. Ind. Electron.*, to be published, doi: 10.1109/TIE.2019.2934021.

[7] Q. Zhong, P. Nguyen, Z. Ma, and W. Sheng, "Self-synchronized synchronverters: Inverters without a dedicated synchronization unit," *IEEE Trans. Power Electron.*, vol. 29, no. 2, pp. 617–630, Feb. 2014.

[8] Z. Shuai, Y. Hu, Y. Peng, C. Tu, and J. Shen, "Dynamic stability analysis of synchronverter-dominated microgrid based on bifurcation theory," *IEEE Trans. Ind. Electron.*, vol. 64, no. 9, pp. 1223–1235, Sep. 2017.

[9] R. Rosso, S. Engelken, and M. Liserre, "Robust stability analysis of synchronverters operating in parallel," *IEEE Trans. Power Electron.*, vol. 34, no. 11, pp. 11309–11319, Nov. 2019.

[10] Z. Shuai, W. Huang, Z. John Shen, A. Luo, and Z. Tian, "Active power oscillation and suppression techniques between two parallel synchronverters during load fluctuations," *IEEE Trans. Power Electron.*, vol. 35, no. 4, pp. 4127–4142, Apr. 2020.

[11] J. Liu, Y. Miura, H. Bevrani, and T. Ise, "Enhanced virtual synchronous generator control for parallel inverters in microgrids," *IEEE Trans. Smart Grid*, vol. 8, no. 5, pp. 2268–2277, Sep. 2017.

[12] J. Alipoor, Y. Miura, and T. Ise, "Stability assessment and optimization methods for microgrid with multiple VSG units," *IEEE Trans. Smart Grid*, vol. 9, no. 2, pp. 1462–1471, Mar. 2018.

[13] Z. Shuai, W. Huang, C. Shen, J. Ge, and J. Shen, "Characteristics and restraining method of fast transient inrush fault currents in synchronverters," *IEEE Trans. Ind. Electron.*, vol. 64, no. 9, pp. 7487–7497, Sep. 2017.

[14] S. Krishnamurthy, T. Jahns, and R. H. Lasseter, "The operation of diesel genset in a CERTS microgrid," in *Proc. IEEE Power Eng. Soc. Conf.*, 2008, pp. 1–8.

[15] R. H. Lasseter and R. Lasseter, "Distributed generation interface to the CERTS microgrid," *IEEE Trans. Power Del.*, vol. 24, no. 3, pp. 1598–1608, Jul. 2009.

[16] Z. Shuai, C. Shen, X. Liu, Z. Li, and Z. Shen, "Transient angle stability of virtual synchronous generators using Lyapunov's direct method," *IEEE Trans. Smart Grid*, vol. 10, no. 4, pp. 4648–4661, Jul. 2019.

[17] J. Liu, Y. Miura, and T. Ise, "Comparison of dynamic characteristics between virtual synchronous generator and droop control in inverter-based distributed generators," *IEEE Trans. Power Electron.*, vol. 31, no. 5, pp. 3600–3611, May 2016.

[18] X. Meng, J. Liu, and Z. Liu, "A generalized droop control for grid-supporting inverter based on comparison between traditional droop control and virtual synchronous generator control," *IEEE Trans. Power Electron.*, vol. 34, no. 6, pp. 5416–5438, Jun. 2019.

[19] P. Hart and B. Lesieutre, "Energy function for a grid-tied, droop controlled inverter," in *Proc. North Amer. Power Symp.*, 2014, pp. 1–6.

[20] H. Xin, L. Huang, L. Zhang, Z. Wang, and J. Hu, "Synchronous instability mechanism of *P-f* droop-controlled voltage source converter caused by current saturation," *IEEE Trans. Power Syst.*, vol. 31, no. 6, pp. 5206–5207, Nov. 2016.

[21] L. Huang, H. Xin, Z. Wang, L. Zhang, K. Wu, and J. Hu, "Transient stability analysis and control design of droop-controlled voltage source converters considering current limitation," *IEEE Trans. Smart Grid*, vol. 10, no. 1, pp. 578–591, Jan. 2019.

[22] M. Kabalan, P. Singh, and D. Niebur, "Nonlinear Lyapunov stability analysis of seven models of a DC/AC droop controlled inverter connected to an infinite bus," *IEEE Trans. Smart Grid*, vol. 10, no. 1, pp. 772–781, Jan. 2019.

[23] A. Paquette, M. Reno, R. Harley, and D. Divan, "Sharing transient loads: Causes of unequal transient load sharing in islanded microgrid operation," *IEEE Ind. Appl. Mag.*, vol. 20, no. 2, pp. 23–34, Dec. 2013.

[24] J. Alipoor, Y. Miura, and T. Ise, "Power system stabilization using virtual synchronous generator with alternating moment of inertia," *IEEE J. Emerg. Sel. Topics Power Electron.*, vol. 3, no. 2, pp. 451–458, Jun. 2015.

[25] N. Soni, S. Doolla, and M. C. Chandorkar, "Improvement of transient response in microgrids using virtual inertia," *IEEE Trans. Power Del.*, vol. 28, no. 3, pp. 1830–1838, Jul. 2013.

[26] F. Katiraei, M. Iravani, and P. Lehn, "Investigation of microgrids with both inverter interfaced and direct AC-connected distributed energy resources," *IEEE Trans. Power Del.*, vol. 26, no. 3, pp. 1634–1642, Jul. 2011.

[27] J. Choi, M. Illindala, A. Mondal, A. Renjit, and M. Pulcherio, "Cascading collapse of a large-scale mixed source microgrid caused by fast-acting inverter-based distributed energy resources," *IEEE Trans. Ind. Appl.*, vol. 54, no. 6, pp. 5727–5735, Nov./Dec. 2018.

[28] A. D. Paquette and D. M. Divan, "Virtual impedance current limiting for inverters in microgrids with synchronous generators," *IEEE Trans. Ind. App.*, vol. 51, no. 2, pp. 1630–1638, Mar./Apr. 2015.

[29] A. H. Etemadi and R. Iravani, "Overcurrent and overload protection of directly voltage-controlled distributed resources in a microgrid," *IEEE Trans. Ind. Electron.*, vol. 60, no. 12, pp. 5629–5638, Dec. 2013.

[30] D. Marx, P. Magne, B. Nahid-Mobarakeh, S. Pierfederici, and B. Davat, "Large signal stability analysis tools in dc power systems with constant power loads and variable power loads: A review," *IEEE Trans. Power Electron.*, vol. 27, no. 4, pp. 1773–1787, Apr. 2012.

[31] P. Magne, D. Marx, B. Nahid-Mobarakeh, and S. Pierfederici, "Large-signal stabilization of a dc-link supplying a constant power load using a virtual capacitor: Impact on the domain of attraction," *IEEE Trans. Ind. App.*, vol. 48, no. 3, pp. 878–887, May/Jun. 2012.

[32] M. Kabalan, P. Singh, and D. Niebur, "Large signal lyapunov-based stability studies in microgrids: a review," *IEEE Trans. Smart Grid*, vol. 8, no. 5, pp. 2287–2295, Sep. 2017.

[33] P. Kundur, *Power System Stability and Control*. New York, NY, USA. McGraw-Hill, 1994.

[34] M. A. Pai. *Energy Function Analysis for Power System Stability*. Norwell, MA, USA: Kluwer, 1989.

Huijie Cheng received the B.S. degree in electrical and information engineering from the Hunan University of Technology, Zhuzhou, China, in 2016. She is currently working toward the Ph.D. degree in electrical engineering with the College of Electrical and Information Engineering, Hunan University, Changsha, China.

Her research interests include stability analysis of the electric traction system and transient stability analysis of the microgrid system.

Zhikang Shuai (Senior Member, IEEE) received the B.S. and Ph.D. degrees from the College of Electrical and Information Engineering, Hunan University, Changsha, China, in 2005 and 2011, respectively, all in electrical engineering.

He was with Hunan University, as an Assistant Professor between 2009 and 2012, and an Associate Professor in 2013. Starting in 2014, he became a Professor with Hunan University. His current research interests include power quality control, power electronics, and microgrid stability analysis and control.

Dr. Shuai was the recipient of the 2010 National Scientific and Technological Awards of China, the 2012 Hunan Technological Invention Awards of China, and the 2007 Scientific and Technological Awards from the National Mechanical Industry Association of China.

Chao Shen received the B.S. degree in electrical and information engineering in 2015 from Hunan University, Changsha, China, where is currently working toward the Ph.D. degree in electrical engineering with the College of Electrical and Information Engineering.

His research interests include mathematical modeling, transient stability analysis, and control of the microgrid system.

Xuan Liu (Member, IEEE) received the B.S. and M.S. degrees from Sichuan University, Chengdu, China, in 2008 and 2011, respectively, and the Ph.D. degree from the Illinois Institute of Technology (IIT), Chicago, IL, USA, in 2015, all in electrical engineering.

He is currently a Professor with the College of Electrical and Information Engineering, Hunan University, Changsha, China. His research interests include smart grid security, operation, and economics of power systems.

Zuyi Li (Senior Member, IEEE) received the B.S. and M.S. degrees from Shanghai Jiaotong University, Shanghai, China, in 1995 and 1998, respectively, and the Ph.D. degree from the Illinois Institute of Technology (IIT), Chicago, IL, USA, in 2002, all in electrical engineering.

He is currently a Professor with the Electrical and Computer Engineering Department, IIT. His research interests include economic and secure operation of electric power systems, cyber security in smart grid, renewable energy integration, electric demand management of data centers, and power system protection.

Z. John Shen (Fellow, IEEE) received the B.S. degree from Tsinghua University, Beijing, China, in 1987, and the M.S. and Ph.D. degrees from Rensselaer Polytechnic Institute, Troy, NY, USA, in 1991 and 1994, respectively, all in electrical engineering.

He was on faculty of the University of Michigan-Dearborn between 1999 and 2004, and the University of Central Florida between 2004 and 2012. He joined the Illinois Institute of Technology in 2013 as the Grainger Chair Professor in electrical and power engineering. He has also held a courtesy professorship with Hunan University, China, since 2007; and with Zhejiang University, China since 2013. His research interests include power electronics, and power semiconductor devices, etc.

Dr. Shen has been an active volunteer in the IEEE Power Electronics Society, and was the VP of Products during 2009–2012, an Associate Editor and Guest Editor-in-Chief of the IEEE TRANSACTIONS ON POWER ELECTRONICS, and the Technical Program Chair and General Chair of several major IEEE conferences.